8.7 A NUMERICAL STUDY OF A NONTORNADIC SUPERCELL OVER FRANCE

Katia Chancibault, V. Ducrocq, J.-P. Lafore*
C.N.R.M., Toulouse, France

1. INTRODUCTION

Observations and numerical studies have significantly increased our understanding of the dynamic of supercell storms, over the past several years. However, a few numerical studies on supercells occurring over Europe, have been carried out.

Our purpose is to improve our understanding of the dynamics of this kind of storm over France by carrying out numerical simulations of one observed case. The under-studied supercell has occurred on 30 May 1999. It has produced strong gust winds, responsible for several casualties and a lot of damage in Paris and its suburbs.

The numerical simulation starts from a large scale operational analysis, and the finest domain uses a 2.5 km horizontal resolution. So that our simulation is close to what is planned by a number of meteorological centers, before the end of this decade, to run operationally.

As our initial state is non-homogeneous, it allows to study the interaction of the supercell dynamics with a low-level discontinuity.

After giving a brief description of the observed storm in the section 2 and of the numerical experiments in section 3, we present an overview of the simulation results in section 4. Finally, we analyze the dynamics leading to the splitting process, in section 5, before concluding in section 6.

2. THE STORM ON 30 MAY 1999

During the night of 29 to 30 may 1999, a first system developed over the near Atlantic Ocean and afterwards progressed inlands. On 30 may 1999, at 04 UTC, the system was nearly 250 km from the south-west of Paris, co-located with the upper-level diffluence associated with the jet exit. At that time, a new system developed on the south-eastern flank of the first system, which was decaying. This second system moved north-eastwards as the mean flow in the upper troposphere.

Two hours later, a splitting process was observed and the issuing right-moving storm reached the suburbs of Paris at 08 UTC (Fig 1). It moved at a speed of about 17 m/s and deviated about 12° from the mean flow. Associated with the right-moving storm, strong winds (more than 110 km/h at different places) and very high rates of precipitation but on very short periods (until 200 mm/h during 5 min) had been recorded. Finally, the right-moving storm began to decay around noon.

The environment of the storm was characterized by a weak convective instability (the proxy sounding at midnight gave values of CAPE around 385 J/kg) in a sheared environment. Convection is also favored by the upper diffluence at the left exit of the jet.

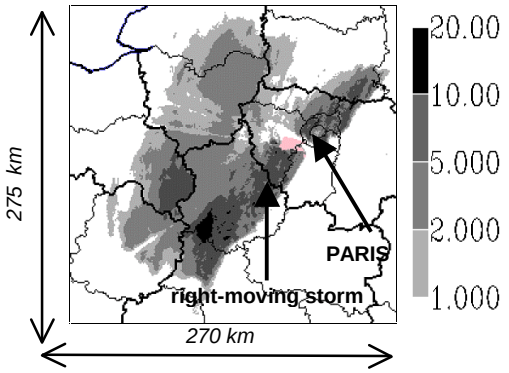

***Fig. 1**: Observed cumulated rainfall over a 3 h 30 period from radar reflectivities. The storm splitting process is showed clearly, with the right-moving storm running over Paris.*

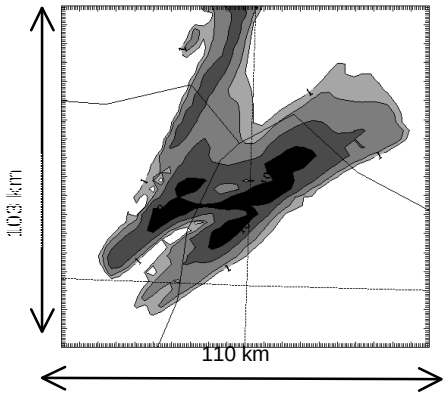

***Fig. 2:** Model cumulated surface rainfall over a 2 h 30 period. Contour intervals are the same as in Fig. 1. The splitting process can been seen with the right-moving storm clearly favored.*

3. MODEL DESCRIPTION

The numerical simulation has been performed with the mesoscale non-hydrostatic model Meso-NH, (Lafore et al, 1998). The simulation used two nested domains, interacting each other according to a two way interactive grid-nesting method (Stein et al, 2000). A cold microphysical scheme governs the

* Corresponding author address: Katia Chancibault, C.N.R.M., Meteo-France, 42, av. Coriolis, 31057 Toulouse, France. E-mail : Katia.Chancibault@meteo.fr

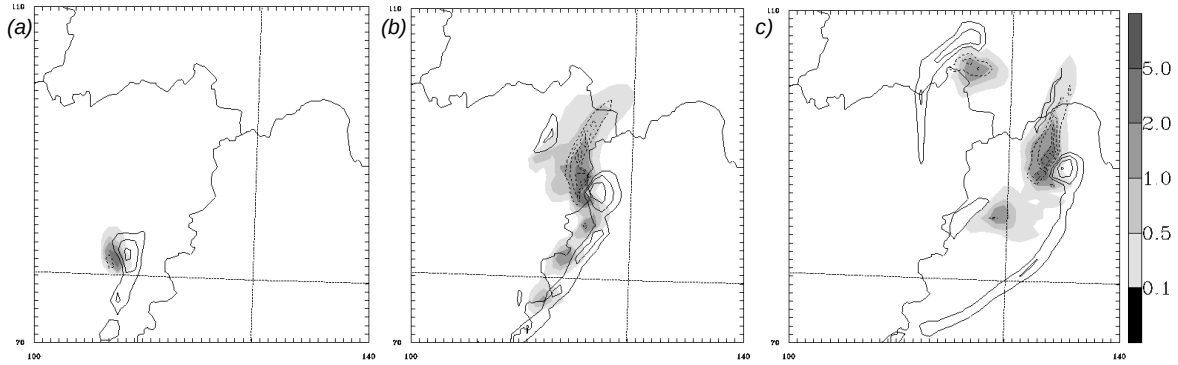

Fig. 3: *Overview of the evolution of the simulated storm with vertical velocities superimposed on the sum of precipitating species mixing ratio, at 1000m after (a) 375 min, (b) 420 min and (c) 480 min of integration. The gray scale of the vertical velocity is given at the right of panel a), in m/s (solid lines for positive values and dashed lines for negative values). The cross-section axes of Fig (d-f) are displayed in thick lines respectively on Fig (a-c). The gray scale of the precipitating hydrometeors in Fig (d-f) is displayed at the right of panel (d) in g/kg. After (a), (d) 375 min; (b), (e) 420 min; (c), (f) 480 min of integration.*

equation of evolution of five hydrometeor species (cloud water, rainwater, primary ice, graupel, snow). In the first model, the horizontal domain is 900×1200 km^2 with 10 km horizontal grid interval. For the fine scale model, the horizontal resolution is of 2.5 km over a 450×360 km^2 domain. A modified version of the Kain and Fritsh scheme (1990) is used as convection parameterization in the outer model, while no convection scheme is utilized in the finest model.

Most of the previous numerical studies have been initialized by horizontally homogeneous fields derived from a proxy or idealized sounding, and a warm or cold bubble is superimposed to trigger the convection. Here, we have chosen to use as initial conditions a large scale operational analysis. Hence, it will exhibit some heterogeneities. No initial disturbance is added. Different large scale analyses as initial state have been tested. Only the simulation starting from the French model ARPEGE analysis at 06 UTC on 30 may 1999 allows to simulate convective cells, with one of these cells leading to a splitting process (Fig. 2). It can be noticed that the simulation starts two hours after the triggering of the observed storm. The model was integrated over a 10 h period.

4. OVERVIEW OF THE SIMULATION

An overview of the evolution of the system is provided in Figure 3, where vertical velocities and the sum of the precipitating species (rainwater + graupel + snow) are displayed. We identify, in the simulation, four stages. First, it is the formation stage, when precipitation forms in the initial storm but does not reach the ground. The initial storm triggers after 300 min of integration, along a mesoscale thermal boundary, on the warm side, inside a convergence line. Then, it moves north-eastward, along the boundary, at a speed of about 16 m/s. Near 360 min, the initial storm enters in its second stage, i.e. the precipitation reaches the ground. Figures 3a show the system at 375 min, in its growing phase, when first surface rainfall appears. The splitting phase begins after 390 min (Fig. 3b). We see two cells separated by an area of downward motions, which is induced by the loading and evaporation of precipitation. Clearly, the right-moving storm is favored. The splitting process lasts about 20 min. After that, the right-moving storm enters in its supercell stage with the typical characteristics of a supercell, as shown for example in the simulations of Wilhelmson & Klemp (1978) or of Rotunno & Klemp (1985): the hook shape is identified in the model reflectivity and the low-level vertical velocities show the low-level upward motions associated with the rear gust front (Fig. 3c)

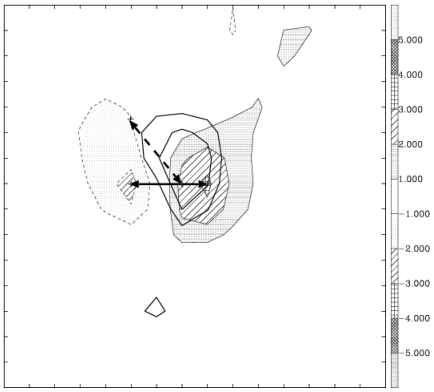

Fig.4 *: Horizontal section at 2000 m of the vertical velocity (the contour lines are for 3 and 5 $m.s^{-1}$) and the vertical vorticity fields (shaded as indicated by the gray scale at the right of the panel, in 10^3 s^{-1}) after 360 min of integration. The continuous double arrow joins the maximum and the minimum of vertical vorticity at 2000m, while the dashed double arrow joins the minimum and the maximum of vertical vorticity at 6000m.*

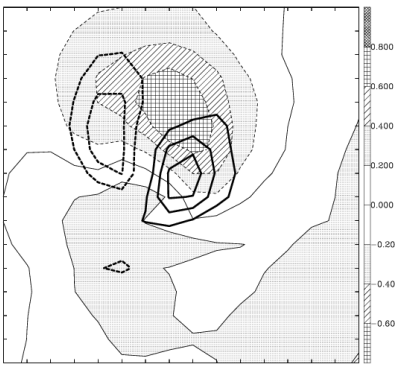

***Fig. 5** : Vertical vorticity (contour lines are in intervals of 10^{-3} s^{-1}; dashed lines indicate negative values; zero lines are omitted) and pressure perturbation field (shaded as indicated at the right of the panel, in hPa) at 5000 m after 360 min. A pressure perturbation couplet can be identified. Its axis is perpendicular to the axis of the vortex pair.*

5. VORTICITY ANALYSIS BEFORE THE SPLITTING PROCESS

We identify clearly a cyclonic vertical vorticity on the right flank of the convective updraft and an anticyclonic vertical vorticity on the left flank (Figure 4). We found, also, as evidenced by Rotunno and Klemp (1982) (see their Figure 4), a pressure perturbation couplet which has its axis perpendicular to the axis of the vortex couplet (Figure 5). The vortex pair axis turns with height (Figure 4), veering of about 50 degrees between 2000 m and 6000 m. However, it can be noticed that the veering with height is not symmetric for the two cores; indeed, the anticyclonic cores undergoes a larger veering between 2000 m and 6000 m than the cyclonic core, which stays approximately at the same location. This dissymmetry is due to the non-homogeneous character of the environment, as it will be shown, hereafter.

Figure 6 presents the low-level conditions, just before the triggering of the initial convective cell. The initial convective cell forms inside a low-level convergence line, materialized by a low-level upward motion line of about 60 km long, in Fig. 6. This upward motion line is located just ahead of a thermal limit, in the warm side, where low-level south-southwestward flow prevails. Hodographs taken in the both sides of the upward line show a different curvature in the low levels, with clockwise shear in the cold side (hodograph B) and an almost straight hodograph in the warm side (hodograph A). The low-level horizontal vorticity vectors have a different direction on each side of the convective cell (Fig. 7a). On the right side, the horizontal vorticity vectors point toward the north, while on the left side, it points westward.

Determination of where the air in both anticyclonic and cyclonic cores originated, was accomplished by calculating backward trajectories (not shown here). They underlines that most of the parcels in the anticyclonic and cyclonic cores originate from the low-level warm side. Some parcels, in the anticyclonic core, come also from the mid-levels of the west side. Tilting, stretching and vertical advection terms of the vertical vorticity equation have been evaluated just before the splitting phase. Where low-level horizontal vorticity vector and vertical velocity gradient vector point in the same direction, the tilting term is positive. Hence, at 1000 m, positive tilting is produced on the east side of the upward motions, due to the southerly horizontal vorticity vector, in the warm side. Some positive tilting is also produced at the north of the updraft, due to the northwesterly horizontal vorticity vectors in the cold side. Significant negative tilting is produced along the west side of the upward motions, due to the northwesterly horizontal vorticity vector, in the cold side. Stretching is located with the upward core and contributes significantly to the positive vertical vorticity (Fig. 7c). On the other hand, the vertical advection of vertical vorticity counter-balances the positive tilting in the west side of the core (Fig. 7e). At 3000 m, the horizontal vorticity field is more homogeneous (Fig 7b). Positive tilting is produced as at 1000 m, in the southeast side of the upward core, while negative tilting core has moved to the northwest side. Stretching and, in a lesser extent, vertical advection tends to attenuate the positive vertical vorticity (Fig. 7d and f). Clearly, the low-level convergence line and the veering of horizontal vorticity vectors, between the warm side and the cold side of the thermal limit, modify, in part, the classic vorticity analysis, carried out by the past, for homogeneous clockwise hodograph.

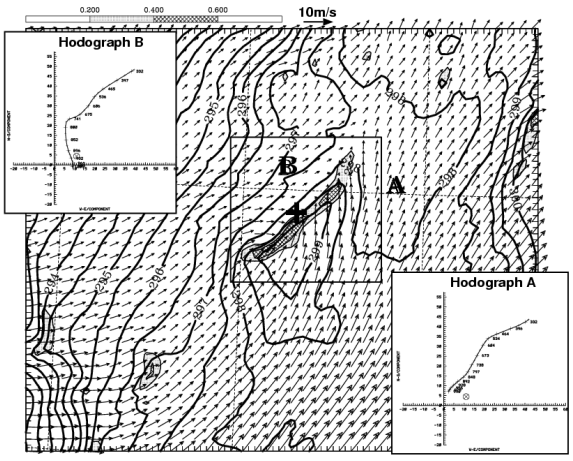

***Fig. 6**: Horizontal section, at 500 m, after 315 min of integration. The contour lines are for virtual potential temperature (contour lines are in intervals of 0.5 ºK), vectors for horizontal wind and gray areas for vertical velocity. Vertical velocity contour intervals and scale for vectors are given at the top of the figure. Letters A and B indicate where the hodographs A and B, respectively, were taken. The cross is for the location of the triggering of the initial convective cell. The box delineates the drawing window of Fig. 7.*

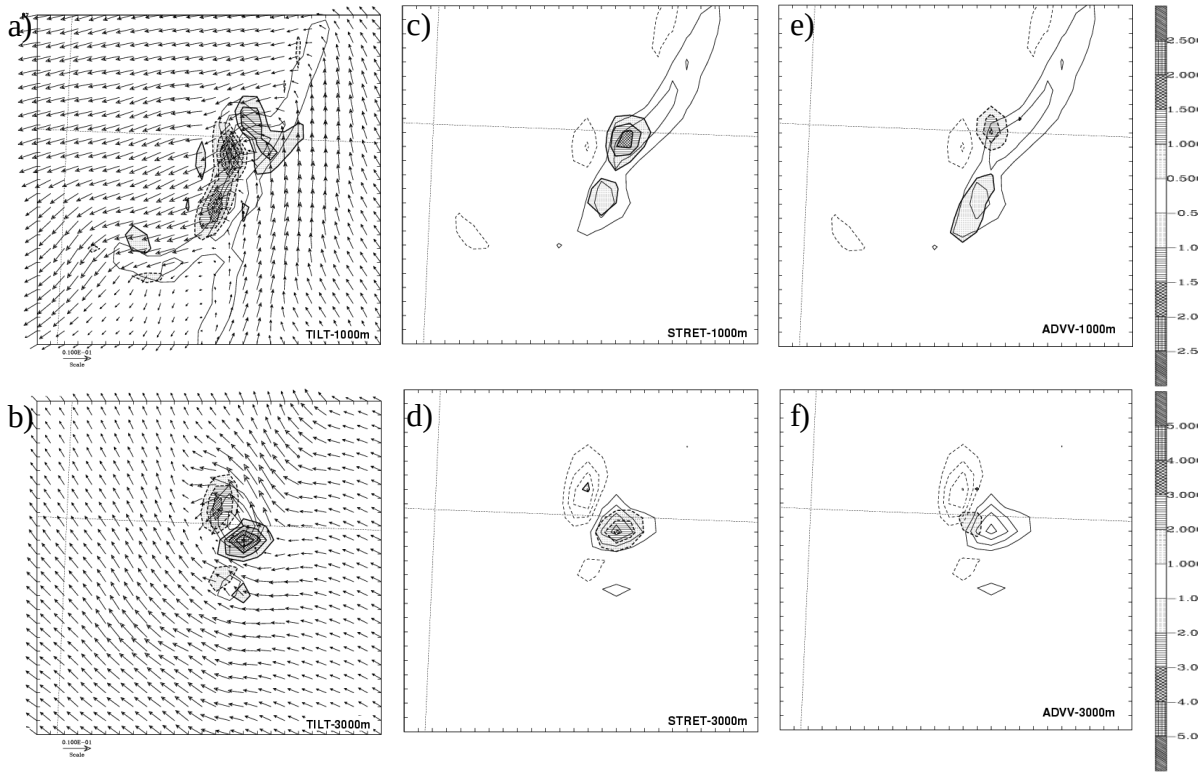

Fig. 7: Distribution of the tilting term at (a) 1000 m and (b) 3000 m, of the stretching term at (c) 1000 m and (d) 3000m and of the vertical advection term at (e) 1000m and (f) 3000 m after 360 min (gray areas scale given at the right of the figure in 10^{-6} s^{-2}). For the panels (a) and (b), the upward vertical velocity at the same height has been superimposed (contour lines of (a) 0.5, 1 and 1.5 $m.s^{-1}$ and (b) 1, 2.5 and 5 $m.s^{-1}$). For panels (c), (d), (e) and (f), the vertical vorticity, at the same height, has been superimposed in solid lines for positive values and in dashed lines for negative values (contour intervals of 0.5 10^{-3} s^{-1}).

7.CONCLUSION

As it has been observed on 30 may 1999, a supercell-like storm produced through a splitting process has been simulated. This has been achieved by starting the model from a non-homogeneous initial state which was provided by a large scale operational analysis.

As in previous numerical studies, which most started from homogeneous initial conditions, four stages leading to the supercell storm are identified and typical characteristics of supercell storm are found in the simulated fields. The analysis performed on the simulated fields of vorticity agrees, partly, with the previous theoretical or numerical studies on the formation of the vorticity couplet, at mid-levels. Differences are found to be related with the non-homogeneous environment.

In the near future, we will complete our analysis by conducting a vorticity analysis during the supercellular stage. Results will be discussed at the conference.

8.REFERENCES

Davies-Jones, R.P., 1984: Streamwise vorticity: the origin of updraft rotation in supercell storms. *J. Atmos. Sci.,* **41**, 2991-3006.

Kain, J.S., and J.M. Fritsch, 1990: A one dimensional entraining/detraining plume model and its application in convective parameterizations. *J. Atmos. Sci.,* **47**, 2784-2802.

Klemp, J.B., and R.B. Wilhelmson, 1978: The simulation of three-dimensional convective storm dynamics. *J. Atmos. Sci.,* **35**, 1070-1096.

Lafore, J.P. *et al.* 1998 : The Meso-NH atmospheric simulation system. Part I: Adiabatic formulation and control simulations. *Ann. Geophysicae,* **16**, 90-109.

Rotunno, R., and J.B. Klemp, 1982: The influence of the shear induced pressure gradient on thunderstorm motion. *Mon. Wea. Rev.,* **110**, 136-151.

Stein, J. *et al.*, 2000: High-resolution non-hydrostatic simulations of flash-flood episodes with grid-nesting and ice-phase parameterization. *Meteor. Atmos. Physics,* **72**, 203-221.

Wilhelmson, R.B., and J.B. Klemp, 1978: A three-dimensional numerical simulation of storm splitting that leads to long-lived storms. *J. Atmos. Sci., **35**, 1974-1986*